

Article

Conversion of Stearic Acid into Bio-Gasoline over Pd/ZSM-5 Catalysts with Enhanced Accessibility

Marta Arroyo ¹, Laura Briones ¹, José María Escola ¹ and David P. Serrano ^{1,2,*}

¹ Group of Chemical and Environmental Engineering, Rey Juan Carlos University, c/ Tulipán s/n, 28933 Móstoles, Madrid, Spain; marta.arroyo@imdea.org (M.A.); laura.briones.gil@urjc.es (L.B.); josemaria.escola.saez@urjc.es (J.M.E.)

² IMDEA Energy Institute, Avda. Ramón de la Sagra, 3, 28935 Móstoles, Madrid, Spain

* Correspondence: david.serrano@imdea.org; Tel.: +34-91-488-70-50

Received: 29 April 2019; Accepted: 6 June 2019; Published: 11 June 2019



Abstract: Palladium supported on nanocrystalline ZSM-5 (n-ZSM-5, Si/Al = 32) and hierarchical ZSM-5 (h-ZSM-5) with different acidity (Si/Al = 33, 51, 122) were tested in the liquid-phase conversion of stearic acid under nitrogen atmosphere (6 bar). The incorporation of Pd into ZSM-5 zeolite increased significantly the share of gasoline in the reaction products due to the promotion by this metal of both decarboxylation and hydrogen transfer reactions. Likewise, the Pd nanoparticles dispersed over the zeolitic support favored the conversion of light olefins formed by end-chain cracking reactions into gasoline-range hydrocarbons according to an oligomerization/cyclization/aromatization pathway. Additionally, Pd/h-ZSM-5 gave rise to higher conversion and selectivity towards gasoline than Pd/n-ZSM-5, due mainly to the enhanced accessibility and improved Pd dispersion achieved when using the hierarchical zeolite. The decrease in the Si/Al atomic ratio in Pd/h-ZSM-5 samples resulted in a rise in the stearic acid conversion, although it was lower than expected. This finding denotes that, for supports with high acid sites concentration, the Pd availability became the limiting factor as the metal was loaded in similar amounts in all catalysts. Finally, the increase of the reaction temperature with the Pd/h-ZSM-5 (122) catalyst augmented both stearic acid conversion and gasoline selectivity, since it enhanced the conversion of the light olefins, formed as primary cracking products, into liquid hydrocarbons. Therefore, it can be concluded that Pd supported on hierarchical ZSM-5 zeolite is a convenient catalyst for obtaining bio-gasoline from oleaginous feedstock.

Keywords: bio-gasoline; stearic acid; Pd; ZSM-5; hierarchical zeolite

1. Introduction

Oleaginous biomass, consisting mainly of triglycerides and fatty acids, is the major component in different products obtained from plants, animals, and microorganisms. Due to their relatively low oxygen content, oleaginous biomass resources are viewed as promising raw materials for obtaining biofuels and/or bio-based chemicals. Accordingly, a number of routes have been developed and investigated for biofuels production from oleaginous biomass, such as transesterification, catalytic cracking, and hydrodeoxygenation.

Fatty acid methyl esters (FAMEs), generated by transesterification of triglycerides with methanol, are known under the conventional denomination of biodiesel and have already reached the commercial scale [1–3]. However, FAMEs present several drawbacks when used in internal combustion engines: high viscosity, low thermal and oxidation stability, and a trend to polymerize, limiting the content of biodiesel up to a maximum of 7 vol% [4,5]. These problems are provoked by the relatively large molecular weight of the triglyceride molecules, as well as by their oxygen content. Therefore, several alternative pathways have been devised to produce fuels from oleaginous biomass

resulting in their transformation into hydrocarbon mixtures, that in terms of both molecular weight and composition, are very similar to petroleum-derived transportation fuels, mainly within the diesel range. These products are usually named as green or renewable diesel to differentiate them from FAME biodiesel and present the advantage of not having any limitations when blending with diesel obtained from petroleum for application in internal combustion engines.

Catalytic cracking of free fatty acids or triglycerides results in gasoline and diesel hydrocarbons. Catalytic cracking of oils under an inert atmosphere has been reported using conventional acid catalysts such as zeolites [6,7], mesoporous aluminosilicates [8], microporous/mesoporous composites [9,10] or bifunctional metallic/acidic catalysts [11]. Typically, catalytic cracking usually proceeds at high temperatures in the vapor phase, which promotes the occurrence of severe cracking reactions and the extensive deposition of coke over the catalyst.

Hydrodeoxygenation of oleaginous feedstocks involves their treatment under moderate temperatures and high hydrogen pressure in order to remove most of their oxygen content, which is released as water. Both the hydrogen consumption and the high pressures required affect quite negatively to the economy of these processes. Hydrodeoxygenation was initially investigated over conventional hydrotreated sulfide catalysts, which have the drawback of requiring a continuous input of sulfur to the reaction medium to remain active [12,13]. Alternatively, the use of transition metals, such as Ni, Mo, Co, W or their combinations, has also been reported [14,15]. Moreover, some interesting results in hydrodeoxygenation processes have been recently disclosed using supported metal phosphide catalysts [16,17].

On the other hand, although quite less investigated, deoxygenation of fatty acids by decarboxylation has been reported over noble metals catalysts (mainly Pd and Pt) [18–20]. Deoxygenation of the feedstock occurs over the metallic phase because the metal accomplishes the preferential adsorption of the fatty acid via the formation of a metal–carboxylate complex along with hydrogen-transfer reactions. A variety of supports have been employed to hike the dispersion of the metal particles in order to increase the exposed surface [21,22]. In this regard, small metal nanoparticles are usually formed over carbonaceous supports, hence, Pd on carbon has become a reference catalyst for free fatty acid decarboxylation [23–25]. More recently, other supports have also been investigated in these types of reactions. In this way, Kubička et al. [12] found that the dispersion of Ni–Mo particles on different supports was as follows: $\text{SiO}_2 > \text{Al}_2\text{O}_3 > \text{TiO}_2$, which led to significant variations in product distribution during the deoxygenation of rapeseed oil. Ford et al. [26] found that the nature of the support modified the preferred route in the deoxygenation of stearic acid over Pd-containing catalysts. Thus, carbon and Al_2O_3 were highly selective for decarboxylation, while SiO_2 led to higher rates of decarbonylation, although with lower activity. Mesostructured silica–aluminas [27–29] and zeolites [30,31] have also been tested in the deoxygenation of fatty acids. In particular, Pd/Al-SBA-15 exhibited a remarkable selectivity toward n-heptadecane in the conversion of stearic acid under a hydrogen atmosphere [32].

In the present work, catalysts consisting of Pd supported over nanocrystalline and hierarchical ZSM-5 zeolites were studied for the liquid-phase transformation of stearic acid into liquid hydrocarbons under mild conditions (temperatures in the range 250–325 °C and 6 bar of nitrogen atmosphere). These supports were chosen because of their strong acidity and convenient accessibility, which was expected to favor the reaction of bulky compounds. In this regard, desilicated hierarchical ZSM-5 displayed in the catalytic fast pyrolysis of biomass enhanced activity for the conversion of bulky oxygenates, resulting in more aromatics and less coke [33]. Additionally, in the catalytic conversion of rapeseed oil, the presence of hierarchical porosity in ZSM-5 augmented the share of light olefins [34]. As is shown below, the combination of acid and Pd centers, as well as convenient accessibility, in the same catalyst led to remarkable activity in the transformation of stearic acid with a remarkable selectivity toward gasoline-range hydrocarbons.

2. Experimental Procedure

2.1. Catalysts Preparation

The hierarchical ZSM-5 supports were synthesized by a protozeolitic units silanization method published in Reference [35], using the following reagents: tetraethylortosilicate (TEOS, 98%, Sigma-Aldrich, St. Louis, LA, USA), tetrapropylammonium hydroxide (TPAOH, Alfa, 40% v/v aqueous solution), aluminum isopropoxide (AIP, Sigma-Aldrich, St. Louis, LA, USA), phenylaminopropyltrimethoxysilane (Sigma-Aldrich, St. Louis, LA, USA), and distilled water. Initially, TPAOH and AIP were dissolved in distilled water and cooled in an ice bath under stirring for several hours until a clear solution was observed. Then, TEOS—previously cooled in ice—was poured dropwise into the solution and left mixing for 1 h. The composition of these mixtures was $x \text{ Al}_2\text{O}_3:60 \text{ SiO}_2:11 \text{ TPAOH}:1500 \text{ H}_2\text{O}$, where x was varied for obtaining Si/Al molar ratios in the gel of 30, 50, and 100, respectively. The solutions were stirred for 40 h at ambient temperature until TEOS was completely hydrolyzed and then the formed ethanol was evaporated in a rotary evaporator at 60 °C. The obtained gels were pre-crystallized at 90 °C for 20 h under reflux to form protozeolitic units. Crystallization was then interrupted by adding 8 mol%, (on a silicon basis) of the silanization agent, keeping the reflux at 90 °C for 6 h. The suspension of silanized units was finally crystallized at 170 °C in an autoclave reactor for 7 days. The obtained solids were removed from the synthesis medium by centrifugation and rinsed with distilled water. Subsequently, they were dried at 110 °C overnight and calcined in static air at 550 °C for 5 h. The materials were called as h-ZSM-5 (X), wherein X stands for their actual Si/Al molar ratio.

Palladium was added on the supports by means of impregnation with a PdCl_2 (99.999%, Aldrich) aqueous solution. The Pd concentration in the solution was adjusted to attain 1 wt % metallic Pd on the final catalysts, employing a ratio (pore volume)/(solution volume ratio) of 1/2. After impregnation, the samples were put in an ultrasonic bath for 30 min and subsequently in a rotary evaporator under vacuum at ambient temperature for 5 h. Finally, they were dried at 110 °C for 12 h and then calcined in a muffle oven at 550 °C for 5 h under static air. Calcined samples were subjected to reduction under 30 mL min^{-1} of H_2 , the temperature increased to 450 °C with a ramp rate of 2 °C min^{-1} and held for 30 min. Subsequently, the samples were cooled down to ambient temperature under N_2 flow. Then, they were stored in a closed vessel under room conditions until being used in reaction.

In order to make proper comparisons, a conventional nanocrystalline ZSM-5 zeolite (Südchemie), named as n-ZSM-5 (32), was also impregnated, characterized, and tested.

2.2. Catalysts Characterization

The samples of the reduced catalysts—Pd as Pd^0 —were characterized using conventional techniques: X-ray diffraction, Inductively-coupled plasma atomic emission spectroscopy (ICP-AES), N_2 and Ar adsorption isotherms, NH_3 TPD (Ammonia temperature programme desorption), and Transmission electron microscopy (TEM). High-angle XRD patterns were taken with a Philips X'PERT MPD diffractometer (Philips, Eindhoven, The Netherlands) using $\text{Cu-K}\alpha$ radiation in order to ascertain the crystallinity of the samples. X-ray diffraction patterns were measured within the $5\text{--}75^\circ$ range employing a step size of 0.1° and a counting time of 10 s. Inductively-coupled plasma atomic emission spectroscopy (Varian, Palo Alto, CA, USA) was employed to determine the Pd content and Si/Al atomic ratio of the samples with a Varian VISTA-AX CCD spectrophotometer. Previously, the samples were digested in a $\text{H}_2\text{SO}_4\text{--HF}$ mixture.

Nitrogen adsorption–desorption isotherms at 77 K were carried out with a Micromeritics TriStar 3000 instrument (Micromeritics, Norcross, GA, USA). The surface areas were calculated by the BET (Brunauer, Emmett, Teller) method using relative pressures in the range 0.05–0.15. Total porosities were determined as the total volume of pores at $P/P_0 = 0.98$. Argon adsorption isotherms at 87 K were performed with a Quantachrome AUTOSORB instrument (Quantachrome, Boynton Beach, FL, USA). Previously, the samples were outgassed at 300 °C for 3 h under vacuum ($P < 10^{-5} \text{ mmHg}$).

The cumulative pore volumes and pore size distributions were determined by the non-local density functional theory (NLDFT) model, assuming cylindrical pore geometry.

Ammonia TPD measurements were performed in a Micromeritics Autochem 2910 apparatus (Micromeritics, Norcross, GA, USA). Initially the samples were heated to 550 °C under a 50 Nml min⁻¹ helium flow, holding this temperature for 30 min. Then, the samples were cooled to 180 °C, and subsequently, a 35 Nml min⁻¹ ammonia flow was circulated for 30 min. Then, the ammonia flow was stopped and a He flow of 50 Nml min⁻¹ was passed through the samples for 90 min. Then, the chemisorbed NH₃ was removed by increasing the temperature to 550 °C with a ramp rate of 15 °C min⁻¹. The ammonia concentration in the effluent gases was monitored by means of a thermal conductivity detector (TCD).

The TEM micrographs were taken in a Philips TECNAI 20 microscope (Philips, Eindhoven, The Netherlands) that operated with a LaB₆ filament under an accelerating voltage of 200 kV. Previously, the samples were prepared by dispersion in acetone, followed by stirring in an ultrasonic bath and final deposition over a carbon-coated copper grid. This technique allows determining the morphology of the support particles as well as the size of the Pd nanoparticles.

2.3. Catalytic Tests of Stearic Acid Conversion

The catalytic experiments were performed in a stainless-steel autoclave furnished with a stirrer and heated by an external oven. In a typical reaction, the corresponding amount of catalyst was loaded (0.4 g) together with 10 wt % stearic acid solution (2 g, 98% Aldrich) in n-dodecane (18 g, ≥99%, Sigma–Aldrich, St. Louis, LA, USA) under 6 bar of nitrogen. Then, the reaction was performed at the desired temperature for a fixed time with stirring. Once the reaction time was reached, the reactor was cooled down to 80 °C. Subsequently, an ice-cooled condenser separated the reaction products into gaseous and liquid fractions which were collected in a gas bag and a vial, respectively. Additionally, the liquid product present in the reactor was collected and separated from the catalyst by filtering under vacuum in a device previously heated to 110 °C.

2.4. Analysis of the Reaction Products

A Varian CP-4900 MicroGC (Varian, Palo Alto, CA, USA) equipped with two injection lines with columns Molsieve 5 Å PLOT and ParaPLOT U/Q, respectively, and TCDs was employed for the analyses of the gaseous phase. Both channels allowed detecting and measuring H₂, CO, CO₂, and hydrocarbons from C₁ to C₄. The liquid products were measured in a Bruker SCIEN 456-GC furnished with a fused silica BR 5 column (0.25 mm internal diameter and 30 m length) and a flame ionization detector (FID). This Gas Chromatography (GC) enabled the separation of compounds in the C₄–C₂₀ interval. Prior to the analyses, the samples were silylated using a method adapted from the EN-14105 standard. For each 0.86 g of sample, 30 µL of pyridine, 90 µL of N-methyl-N-(trimethylsilyl)-trifluoroacetamide (MSTFA), and 10 µL of 1,2,3,4-tetrahydronaphthalene as internal standard were mixed and strongly shaken. This mixture was held at ambient temperature for 15 min before analysis.

3. Results and Discussion

3.1. Catalysts Properties

This section discloses the main features of the supports and catalysts employed in this work. Two different types of ZSM-5 zeolites were used as support of the Pd nanoparticles: nanocrystalline and hierarchical ZSM-5 zeolites, named as n-ZSM-5 and h-ZSM-5, respectively. For the hierarchical zeolitic supports, several samples were prepared having different Si/Al atomic ratios (~33–122). Regarding the Pd content, all catalysts presented an amount of this metal slightly lower than the theoretically loaded (1 wt %), with some deviation being observed for the Pd/n-ZSM-5 (32) catalyst, with a Pd amount of 0.84 wt %, which could indicate a lower association of the Pd moieties with the nanocrystalline zeolitic support during the impregnation treatment.

Figure 1 displays the high-angle XRD patterns of the reduced Pd catalysts. All the samples exhibited the typical XRD patterns of MFI zeolite, with no trace of amorphous material. Only in the case of the Pd/h-ZSM-5 (33) were less intense reflections appreciated, which suggests the occurrence of smaller crystalline domains in this sample. Despite the low amount of Pd loaded (around 1 wt %), the reflection of Pd metal at $2\theta \sim 40.1^\circ$ (marked with an asterisk) may be observed in all the catalysts in a similar way, bearing out the presence of this metal.

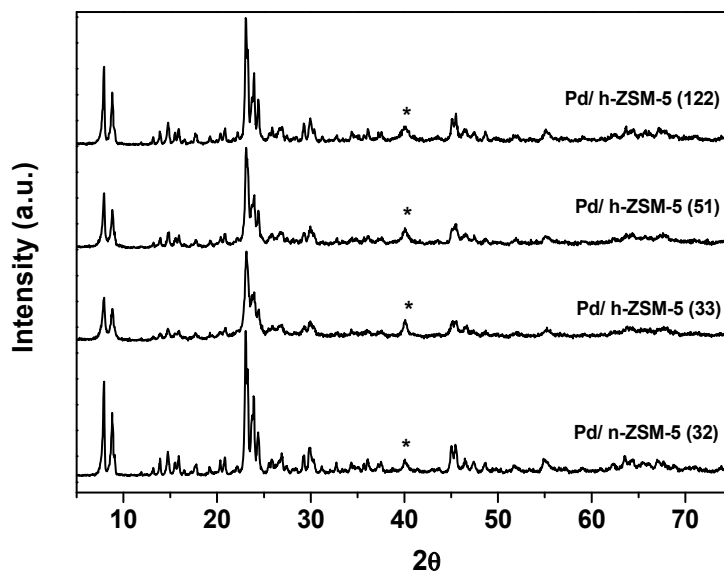


Figure 1. X-ray diffraction patterns of the Pd/ZSM-5 catalysts.

Figure 2 exhibits the Ar adsorption–desorption isotherms of both carriers and Pd-containing materials. In addition to the adsorption occurring at low relative pressures, arising from the zeolite micropores, the samples also exhibited significant Ar uptake and intermediate relative pressure, which was consistent with the respective nanocrystalline and hierarchical features of the zeolitic supports. In all cases, the incorporation of Pd caused some decreases in the adsorption capacity of the supports. This finding can be assigned to the occurrence of some micro- and mesopore blocking caused by the deposition of the Pd nanoparticles and/or to some contraction of the mesoporosity provoked by the thermal treatment of hydrogen reduction at high temperature (450 °C). On the other hand, almost no hysteresis was appreciated in the desorption branch of the isotherm indicating the absence of bottle-neck pores.

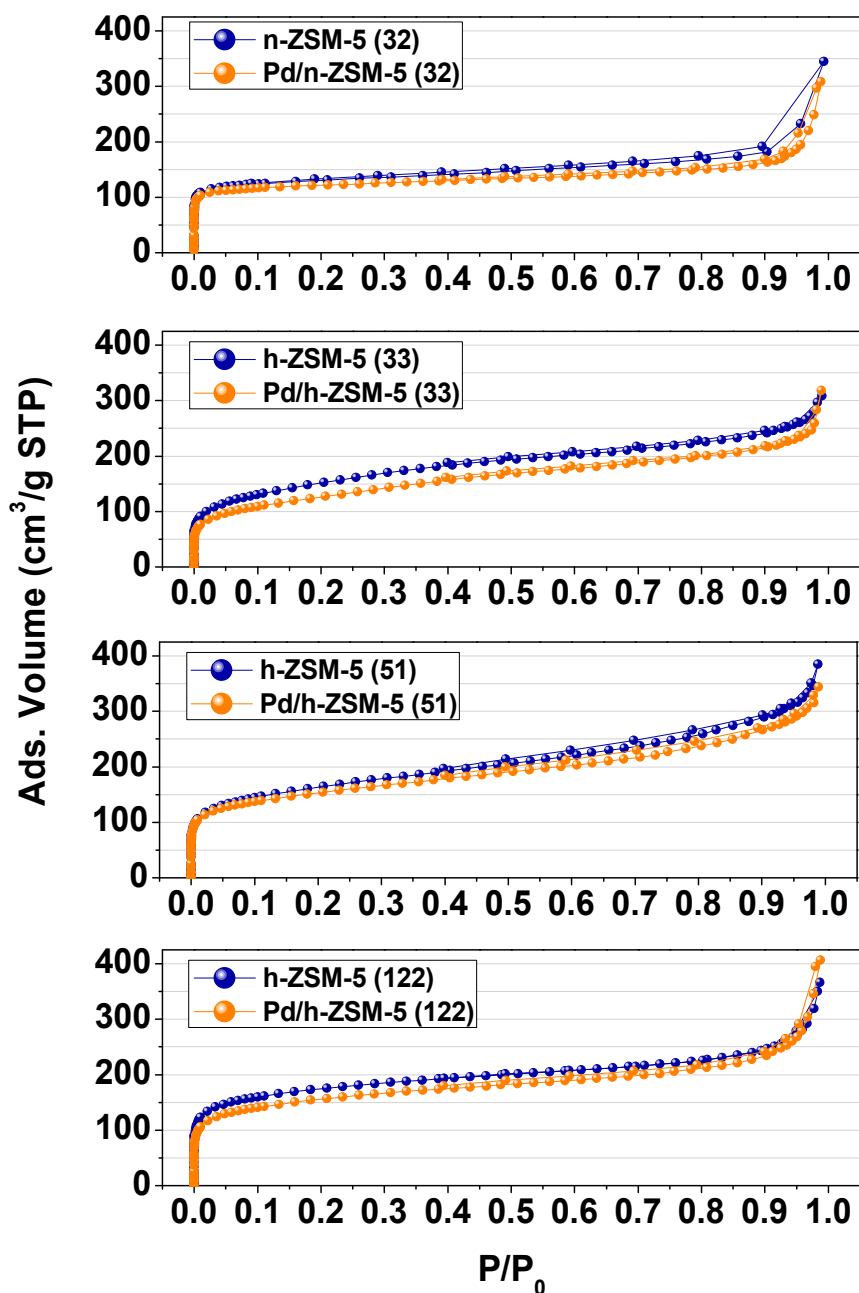


Figure 2. Ar adsorption–desorption isotherms at 87 K of both the Pd/ZSM-5 catalysts and the corresponding supports.

As inferred from Table 1, the hierarchical Pd/h-ZSM-5 catalysts, irrespective of their Si/Al atomic ratio, showed enhanced textural properties with regard to Pd/n-ZSM-5 (32), with superior BET surface areas ($\sim 100 \text{ m}^2 \text{ g}^{-1}$ above) and pore volumes ($>0.04\text{--}0.120 \text{ cm}^3 \text{ g}^{-1}$). On the contrary, the sample based on the nanocrystalline ZSM-5 support exhibited the highest micropore surface ($274 \text{ m}^2 \text{ g}^{-1}$) and the lowest external/mesopore surface area ($103 \text{ m}^2 \text{ g}^{-1}$). For the hierarchical Pd/h-ZSM-5 catalysts, an influence of the Si/Al atomic ratio over the micropore and external/mesopore surface area may be observed. In this regard, the micropore surface area decreased at lower Si/Al atomic ratios, while the contrary was appreciated for the external/mesopore surface area. The great proportion of external/mesopore surface areas in all the samples, and in particular for the catalysts prepared from hierarchical ZSM-5 supports, confirms their high accessibility for the reaction of large molecules, such as stearic acid.

Table 1. Physicochemical properties of the catalysts.

Sample	Pd/n-ZSM-5 (32)	Pd/h-ZSM-5 (33)	Pd/h-ZSM-5 (51)	Pd/h-ZSM-5 (122)
Si/Al Molar Ratio	32	33	51	122
Pd Content (wt %)	0.84	0.96	0.91	0.94
Pd Mean Size (nm)	23	13	14	17
BET Surface Area (m ² g ⁻¹)	377	477	479	486
Total Pores Volume (cm ³ g ⁻¹)	0.434	0.497	0.471	0.557
Micropores Volume (cm ³ g ⁻¹)	0.171	0.130	0.157	0.165
Micropore Surface Area (m ² /g)	274	209	252	265
External/Mesopores Surface Area (m ² /g)	103	268	227	221
Tmax NH ₃ Desorption (°C)	330	340	340	332
Acidity (meq NH ₃ g ⁻¹)	0.345	0.305	0.242	0.122

The acid properties of the catalysts were calculated by means of ammonia TPD measurements and their results are summarized in Table 1. Pd/n-ZSM-5 (32) presents a higher content of strong acid sites than Pd/h-ZSM-5 (33). For the hierarchical Pd/h-ZSM-5 catalysts, when the Si/Al atomic ratios increased, there was a parallel abatement in the total acidities, while their strength was fairly similar, according to their respective maximum temperature of ammonia desorption. The acid properties of the Pd-containing catalysts were fairly similar to those of the original supports, which can be found elsewhere [36], with only slight variations in the overall acidity being observed.

Figure 3 illustrates TEM micrographs of the Pd-containing catalysts. The Pd/n-ZSM-5 (32) was constituted by agglomerates of nanounits with sizes in the range 40–100 nm. The materials based on hierarchical zeolitic supports presented a sponge-like aspect, being formed by aggregates (200–400 nm) of very small zeolitic nanounits (5–10 nm). In all cases, the presence of Pd nanoparticles deposited over the external surface of the zeolite crystals or located within the aggregates was clearly observed. As inferred from Table 1, the average size of the Pd nanoparticles, determined from the TEM images, was lower for the catalysts prepared from the hierarchical support compared to that of the nanocrystalline ZSM-5, denoting that the mesoporosity present in the former led to a better dispersion of the metal, as it has been earlier reported [36]. Likewise, increasing the Si/Al ratio of the hierarchical zeolitic supports led to progressively larger Pd nanoparticles. Therefore, it can be concluded that the presence of Al in the hierarchical supports afforded a better Pd dispersion.

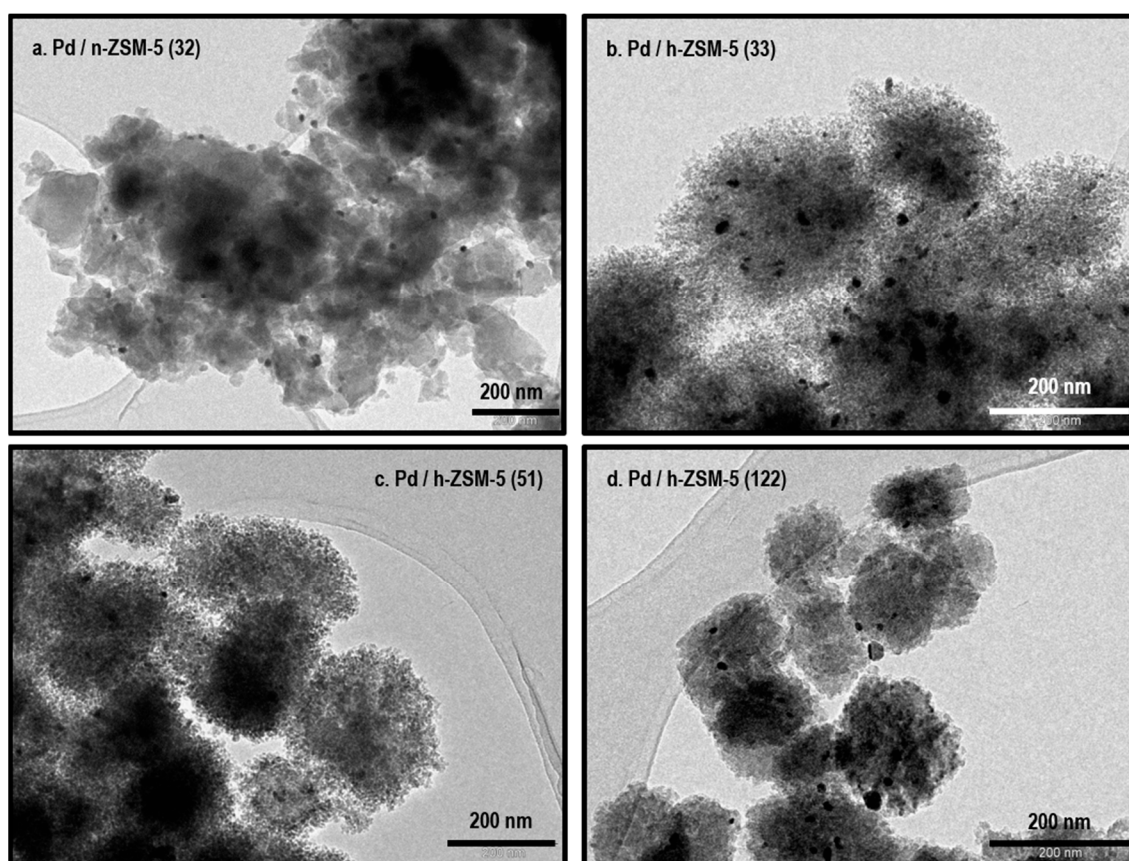


Figure 3. TEM micrographs of the Pd/h-ZSM-5 samples. (a) Pd/n-ZSM-5 (32); (b) Pd/h-ZSM-5 (33); (c) Pd/h-ZSM-5 (51); (d) Pd/h-ZSM-5 (122).

3.2. Reactions of Stearic Acid

3.2.1. Effect of the Pd Incorporation

Initially, tests of stearic acid conversion were performed comparing the parent nanocrystalline n-ZSM-5 and Pd/n-ZSM-5 catalysts to ascertain the role played by the addition of the metal. As illustrated in Figure 4, almost complete conversion of stearic acid into hydrocarbons was attained over both catalysts, showing the high decarboxylation activity of these materials under the employed operation conditions ($T = 325\text{ }^{\circ}\text{C}$, 6 bar of N_2). Regarding the hydrocarbon distribution (Figure 5), the main products obtained were gases and gasoline range compounds. The main components in the gases are C_3 and C_4 olefins, proceeding from end-chain cracking reactions of the carbocations species formed by stearic acid decarboxylation. On the other hand, two pathways can be envisaged to explain the formation of gasoline range hydrocarbons: i) random cracking reactions at any position in the chain of those carbocations, and ii) oligomerization/cyclization/aromatization (OCA pathway) of the light olefins formed by severe cracking reactions. Both end-chain cracking and OCA pathways are known to occur on the acid sites of the ZSM-5 zeolite [37–39]. Interestingly, the addition of Pd to the n-ZSM-5 support results in the production of less gaseous hydrocarbons and more gasoline. Moreover, the carbon atom distribution obtained over the Pd-containing catalyst exhibited a more regular profile, whereas the selectivity towards gasoline-range hydrocarbons increased from 65.5% over the n-ZSM-5 (32) sample up to 77.5% when using the Pd/n-ZSM-5 (32) catalyst. This positive finding can be assigned to a promotion effect of the OCA pathway provoked by the Pd species. In this way, Pd is known to present activity in the oligomerization and polymerization of olefins [40–43], which would be in agreement with its participation also in olefin oligomerization reactions. Moreover, Pd exhibits hydrogen transfer activity, which could favor the aromatization step in the OCA pathway [44–47].

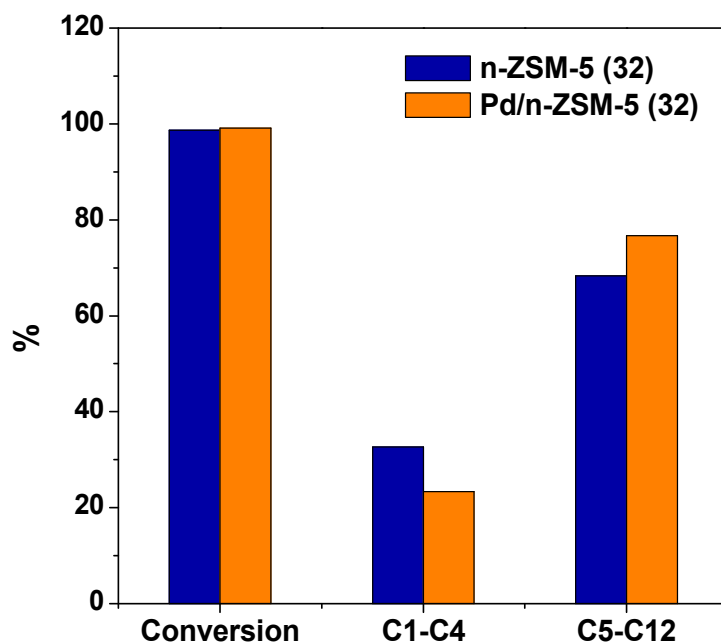


Figure 4. Stearic acid conversion and selectivity by groups over the Pd/n-ZSM-5 (32) and n-ZSM-5 (32) samples ($T = 325\text{ }^{\circ}\text{C}$).

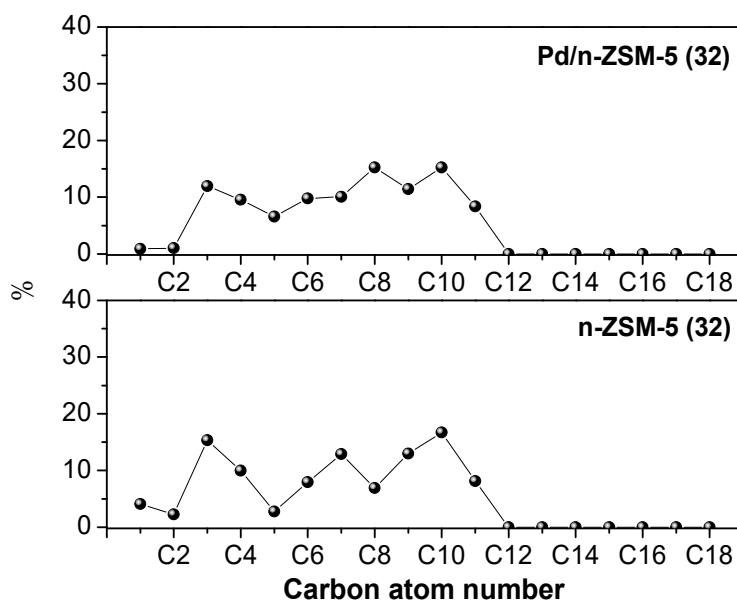


Figure 5. Selectivity by atom carbon number over the Pd/n-ZSM-5 (32) and n-ZSM-5 (32) samples ($T = 325\text{ }^{\circ}\text{C}$).

3.2.2. Influence of the Hierarchical Porosity

With the goal of assessing the effect of the presence of hierarchical porosity in the zeolitic support, Pd/n-ZSM-5 (32) and Pd/h-ZSM-5 (33) catalysts were tested and compared in the conversion of stearic acid. Figure 6 shows the conversion and selectivities by groups to the different products so obtained over both catalysts. A quite higher activity was exhibited by Pd/h-ZSM-5 (33) with regards to Pd/n-ZSM-5 (32), with values of the stearic acid conversion of 67 and 33%, respectively. Since both materials present similar acid properties, this remarkable difference can be related to the presence of the hierarchical porosity, which increases the accessibility of the zeolite acid sites and enhances the dispersion of the Pd nanoparticles over the zeolitic support.

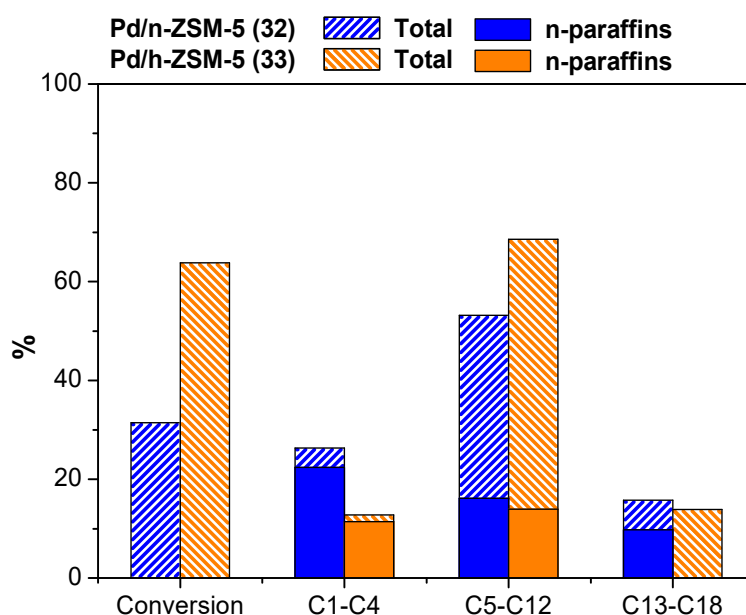


Figure 6. Stearic acid conversion and selectivity by groups over the Pd/n-ZSM-5 (32) and Pd/h-ZSM-5 (33) samples ($T = 300\text{ }^{\circ}\text{C}$).

Regarding the product distribution, and under the conditions employed in these experiments, diesel range hydrocarbons with selectivity around 15% were also produced over both catalysts, in addition to the gases and gasoline fractions. Interestingly, the use of the hierarchical zeolitic support also led to a remarkable improvement in the gasoline selectivity (72 over Pd/h-ZSM-5 (33) versus 56% when using the Pd/n-ZSM-5 (32) catalyst). This result can be mainly related to the improved Pd dispersion and enhanced accessibility through its mesopores over the hierarchical ZSM-5 sample, which favors the OCA pathway by increasing the closeness between acid and metallic sites and by enhancing hydrogen transfer reactions.

Therefore, the addition of a secondary porosity within the mesopore range in the ZSM-5 support had a paramount influence on the behavior of the corresponding catalyst in stearic acid conversion, leading to remarkable enhancements in both catalytic activity and selectivity towards gasoline range hydrocarbons.

3.2.3. Effect of the Si/Al Atomic Ratio in Hierarchical ZSM-5

The Si/Al atomic ratio of the zeolitic ZSM-5 materials is a key variable, since it determines the acid concentration, which is meant to play a decisive role in the stearic acid conversion and the obtained product distribution. To determine the effect of this parameter, three Pd/h-ZSM-5 samples, with Si/Al atomic ratios of 33, 51, and 122, were assessed as catalysts of this reaction. The attained conversions and selectivity by groups are shown in Figure 7, while the selectivity by atom carbon number is illustrated in Figure 8. It can be appreciated that decreasing the Si/Al ratio provoked an improvement of the stearic acid conversion, but this was not as significant as it might be expected. Thus, a three-fold increase in the aluminum content did not even double the attained conversion. Moreover, it was remarkable the high conversion of stearic acid obtained over Pd/h-ZSM-5 (122) (47%), despite its low acidity. Additionally, if the textural properties of these three catalysts are compared, the catalyst with the highest accessibility (higher mesopore surface area/ lowest micropore surface area) is also the sample with the lowest Si/Al atomic ratio (Pd/h-ZSM-5 (33)). Therefore, considering its enhanced properties, it should provide a much higher conversion than that observed (68%), if only accessibility and aluminum content were responsible for the attained conversions. This fact bears out the relevant role also played by the Pd species, contributing significantly to the decarboxylation activity. Moreover, as all the samples contained similar Pd amounts, the availability of the Pd centers

may become the limiting factor for the conversion of stearic acid when using catalysts with high acid sites concentration.

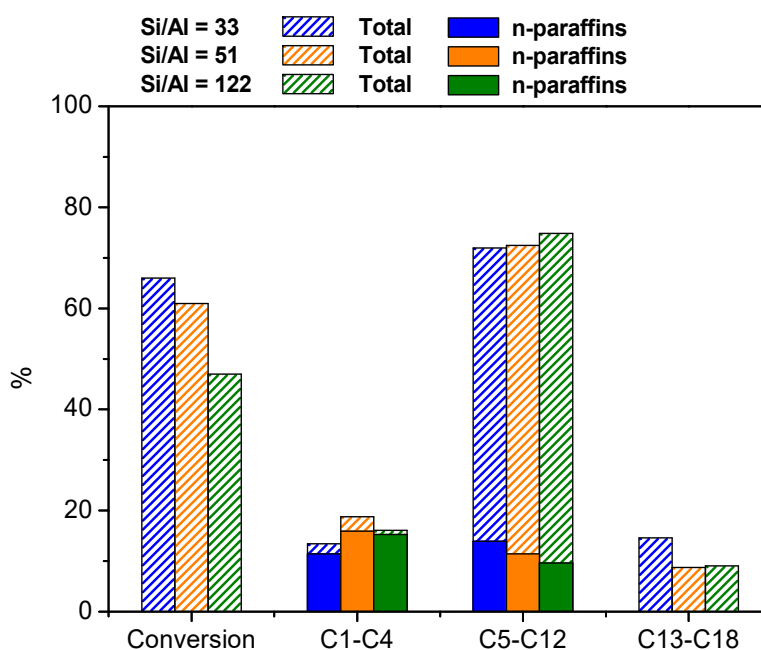


Figure 7. Stearic acid conversion and selectivity by groups over Pd/h-ZSM-5 catalysts with different Si/Al ratios (T = 300 °C).

Regarding the product distribution, the three catalysts gave rise to selectivities towards gasoline-range hydrocarbons above 70%, with a slight increase being observed as the acidity of the support was reduced. On the other hand, the selectivity to n-paraffins was lower than 30%, regardless of the used Si/Al atomic ratio. Regarding the selectivity by carbon atom number, it was interesting to observe how the main hydrocarbon fraction obtained at the lowest Si/Al atomic ratios (33 and 51) was C₅, while for the highest Si/Al atomic ratio, it was C₈, and to a lesser extent, C₁₁. This fact suggests also that the OCA pathway is promoted by the presence of Pd, this effect becoming more evident when using zeolite catalysts with low Al contents, i.e., high Pd/Al ratios. In contrast, at low Pd/Al ratios, the end-chain cracking reactions take place in a higher extent than the OCA pathway, explaining that lighter hydrocarbons are predominant in the product distribution

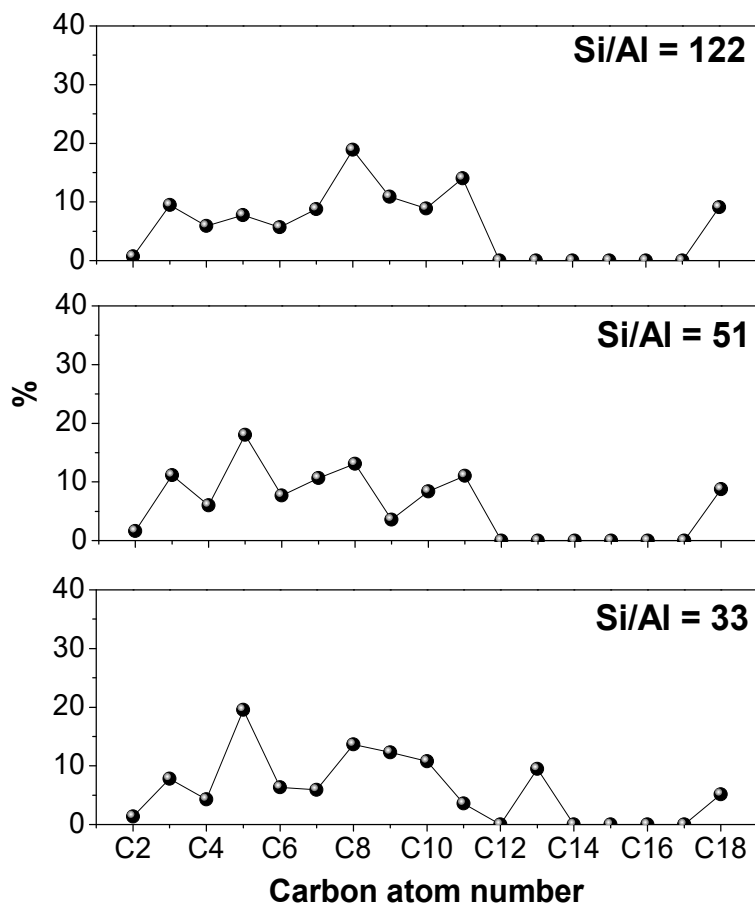


Figure 8. Influence of the Si/Al atomic ratio of the Pd/h-ZSM-5 catalysts over the selectivity by atom carbon number ($T = 300\text{ }^{\circ}\text{C}$).

3.2.4. Effect of the Reaction Temperature over Hierarchical ZSM-5

The effect of the temperature on the stearic acid conversion was determined over the Pd/h-ZSM-5 (122) catalyst by operating at 250, 275, 300, and 325 °C. Figure 9 illustrates the conversion and selectivities by groups so obtained, whereas Figure 10 shows the corresponding selectivities by carbon atom.

At the lowest temperature (250 °C), the conversion was very low (6%) and the product comprised solely C₂–C₄ hydrocarbons. With the increase in temperature, a strong enhancement of the stearic acid conversion took place, reaching almost total conversion at 325 °C. This confirms the high activity of the catalytic system here investigated, although some contribution of the thermal reaction cannot be discarded when working at the highest temperature.

It is noteworthy that the selectivity towards C₁–C₄ hydrocarbons dropped steadily with temperature, until reaching a minimum value of 12% at 325 °C. In the same way, the selectivity to products within the diesel was reduced when working at higher temperature. As a consequence, the selectivity towards the gasoline fraction was significantly improved with the temperature, rising from 46% at 275 °C to a remarkable value of 86% at 325 °C.

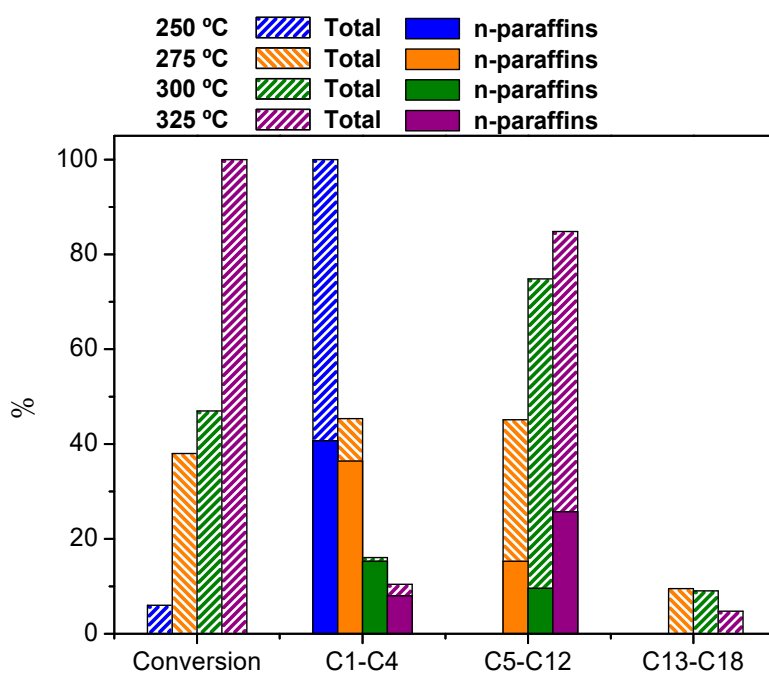


Figure 9. Effect of the reaction temperature on the stearic acid conversion and selectivity by groups over the Pd/h-ZSM-5 (122).

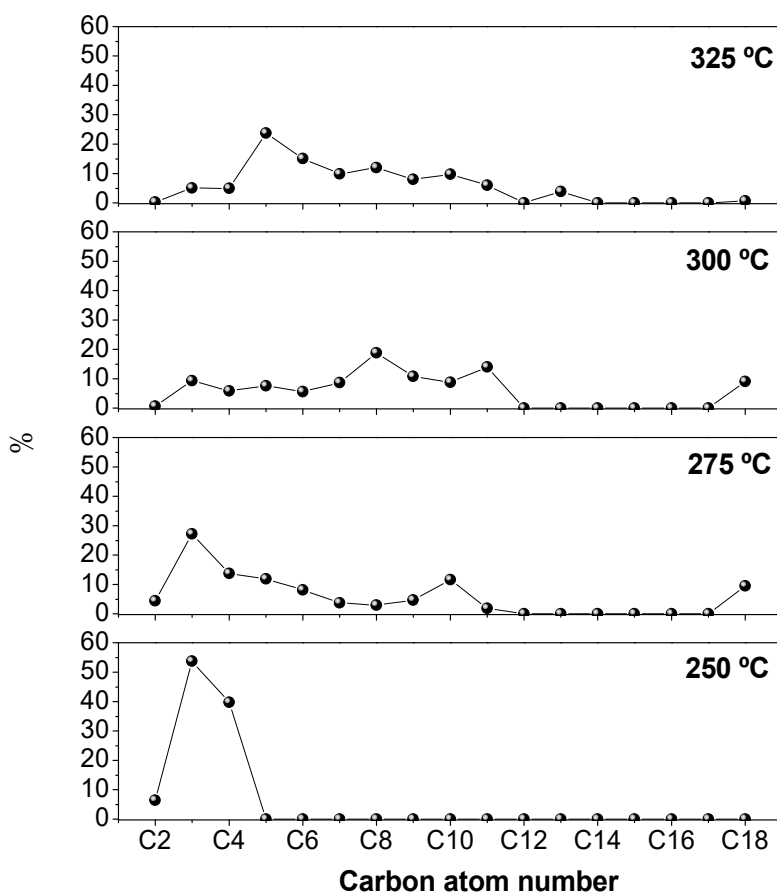


Figure 10. Effect of the reaction temperature on the selectivity by atom carbon number in the stearic acid conversion over the Pd/h-ZSM-5 (122) catalyst.

Regarding the selectivity by carbon atom, shown in Figure 9, the main hydrocarbon obtained was C₃ at 250 and 275 °C, changing to C₈ and C₁₁ at 300 °C. The selectivity towards n-paraffins in the C₅–C₁₂ fraction was mostly 26% at 325 °C and lower at 250 and 275 °C, pointing out that the main components of this bio-gasoline were branched, naphthenes, and aromatic hydrocarbons formed as a consequence of isomerization, cyclization, and aromatization reactions. The enhanced relevance of the OCA pathway was revealed by the relatively plain product distribution obtained in terms of atom carbon number when increasing the reaction temperature up to 300 °C.

In summary, these results indicate that by adjusting the properties of the ZSM-5 support, as well as the operation conditions, it is possible to achieve almost total conversion of stearic acid with a high selectivity towards gasoline-range hydrocarbons.

4. Conclusions

Palladium supported over either nanocrystalline or hierarchical ZSM-5 samples showed remarkable properties for liquid-phase conversion of stearic acid into liquid fuels using mild reaction temperatures under nitrogen atmosphere. These catalysts exhibited high selectivity towards gasoline-range hydrocarbons, plus an additional share of gaseous components produced by end-chain cracking reactions. The occurrence of Pd in the catalyst composition led towards an increase in the gasoline selectivity, due to the higher extent of the oligomerization/cyclization/aromatization pathway (OCA), which promoted the conversion of the light olefins, formed as primary end-chain cracking products.

When using ZSM-5 supports with hierarchical porosity, both stearic acid conversion and gasoline selectivity were significantly improved. These facts were caused by the enhanced accessibility and better Pd dispersion attained over the hierarchical zeolites in respect to the Pd/n-ZSM-5 catalyst. It is also noteworthy that the increase of the Al content in the hierarchical Pd/h-ZSM-5 catalysts brought about a lower increase in conversion than the expected one, considering the rise of the zeolite acid site concentration. This fact was indicative of the critical role played by the Pd species in the activity of the catalysts, suggesting that the availability of the Pd centers may become a limiting factor in the conversion of stearic acid.

The enhancement of the reaction temperature increased the stearic acid conversion, reaching virtually complete conversion at 325 °C. Interestingly, the selectivity towards gasoline underwent a high increase with this variable, from 46% at 275 °C to a superb value of 86% at 325 °C. This phenomenon was explained in terms of a larger extent of the OCA pathway.

Accordingly, by adjusting the zeolitic support properties and operation conditions, it is possible to achieve Pd/ZSM-5 catalysts showing both high catalytic activity and selectivity for the conversion of fatty acids (stearic acid) into bio-gasoline.

Author Contributions: Conceptualization, D.P.S.; methodology, M.A. and L.B.; software, M.A. and L.B.; validation, J.M.E.; formal analysis, M.A. and L.B.; investigation, M.A.; resources, L.B.; data curation, M.A.; writing—original draft preparation, J.M.E.; writing—review and editing, D.P.S.; visualization, D.P.S.; supervision, D.P.S.; Project administration, D.P.S. and J.M.E.; funding acquisition, D.P.S. and J.M.E.

Funding: This research was funded by Ministry of Economics and Competitiveness of Spain, grant number CTQ2014-60209-R.

Conflicts of Interest: The authors declare no conflict of interest.

References

1. Meher, L.C.; Vidya Sagar, D.; Naik, S.N. Technical aspects of biodiesel production by transesterification—a review. *Renew. Sustain. Energy Rev.* **2006**, *10*, 248–268. [[CrossRef](#)]
2. Leung, D.Y.C.; Wu, X.; Leung, M.K.H. A review on biodiesel production using catalyzed transesterification. *Appl. Energy* **2010**, *87*, 1083–1095. [[CrossRef](#)]
3. Mata, T.M.; Martins, A.A.; Caetano, N.S. Microalgae for biodiesel production and other applications: A review. *Renew. Sustain. Energy Rev.* **2010**, *14*, 217–232. [[CrossRef](#)]

4. Zhao, C.; Brück, T.; Lercher, J.A. Catalytic deoxygenation of microalgae oil to green hydrocarbons. *Green Chem.* **2013**, *15*, 1720–1739. [[CrossRef](#)]
5. Benjumea, P.; Agudelo, J.; Agudelo, A. Basic properties of palm oil biodiesel—Diésel blends. *Fuel* **2008**, *87*, 2069–2075. [[CrossRef](#)]
6. Corma, A.; Huber, G.W.; Sauvanaud, L.; O'Connor, P. Processing biomass derived oxygenates in the oil refinery: Catalytic cracking (FCC) reaction pathways and role of catalyst. *J. Catal.* **2007**, *247*, 307–327. [[CrossRef](#)]
7. Huber, G.W.; Corma, A. Synergies between bio- and oil refineries for the production of fuel from biomass. *Angew. Chem. Int. Ed.* **2007**, *46*, 7184–7201. [[CrossRef](#)]
8. Twaiq, F.A.; Mohamed, A.R.; Bhatia, S. Liquid hydrocarbon fuels from palm oil by catalytic cracking over aluminosilicate mesoporous catalysts with various Si/Al ratios. *Microporous Mesoporous Mater.* **2003**, *64*, 95–107. [[CrossRef](#)]
9. Katikaneni, S.P.R.; Adjaye, J.D.; Bakhshi, N.N. Studies on the catalytic conversion of canola oil to hydrocarbons: Influence of the hybrid catalysts and steam. *Energy Fuels* **1995**, *9*, 599–609. [[CrossRef](#)]
10. Ooi, Y.-S.; Zakaria, R.; Mohamed, A.R.; Bhatia, S. Catalytic conversion of fatty acids mixture to liquid fuel and chemicals over composite microporous/mesoporous catalysts. *Energy Fuels* **2005**, *19*, 736–743. [[CrossRef](#)]
11. Danuthai, T.; Jongpatiwut, S.; Rirksomboon, T.; Osuwan, S.; Resaco, R.E. Conversion of methylesters to hydrocarbons over Zn-modified HZSM-5 zeolite catalyst. *Catal. Lett.* **2009**, *132*, 197–204. [[CrossRef](#)]
12. Kubička, D.; Kaluža, L. Deoxygenation of vegetable oils over sulfided Ni, Mo and NiMo catalysts. *Appl. Catal. A* **2010**, *372*, 199–208. [[CrossRef](#)]
13. Toba, M.; Abe, Y.; Kuramochi, H.; Osako, M.; Mochizuki, T.; Yoshimura, Y. Hydrodeoxygenation of waste vegetable oil over sulfide catalysts. *Catal. Today* **2011**, *164*, 533–537. [[CrossRef](#)]
14. Ochoa-Hernández, C.; Yang, Y.; Pizarro, P.; de la Peña O'Shea, V.A.; Coronado, J.M.; Serrano, D.P. Hydrocarbons production through hydrotreating of methyl esters over Ni and Co supported on SBA-15 and Al-SBA-15. *Catal. Today* **2013**, *210*, 81–88. [[CrossRef](#)]
15. Boda, L.; Onyestyák, G.; Solt, H.; Lóny, F.; Valyon, J.; Thernes, A. Catalytic hydroconversion of tricaprolylin and caprylic acid as model reaction for biofuel production from triglycerides. *Appl. Catal. A* **2010**, *374*, 158–169. [[CrossRef](#)]
16. Berenguer, A.; Bennett, J.A.; Hunns, J.; Moreno, I.; Coronado, J.M.; Lee, A.F.; Pizarro, P.; Wilson, K.; Serrano, D.P. Catalytic hydrodeoxygenation of m-cresol over Ni₂P/hierarchical ZSM-5. *Catal. Today* **2018**, *304*, 72–79. [[CrossRef](#)]
17. Dierks, M.; Cao, Z.; Manayil, J.C.; Akilavasan, J.; Wilson, K.; Schüth, F.; Rinaldi, R. Impact of hydrophobic organohybrid silicas on the stability of Ni₂P catalysts phase in the hydrodeoxygenation of biophenols. *ChemCatChem* **2018**, *10*, 2219–2231. [[CrossRef](#)]
18. Snåre, M.; Kubickova, I.; Mäki-Arvela, P.; Murzin, D.Y. Heterogeneous catalytic deoxygenation of stearic acid for production of biodiesel. *Ind. Eng. Chem. Res.* **2006**, *45*, 5708–5715. [[CrossRef](#)]
19. Ping, E.W.; Pierson, J.; Wallace, R.; Miller, J.T.; Fuller, T.F.; Jones, C.W. On the nature of the deactivation of supported palladium nanoparticle catalysts in the decarboxylation of fatty acids. *Appl. Catal. A* **2011**, *396*, 85–90. [[CrossRef](#)]
20. Madsen, A.T.; Rozmysłowicz, B.; Simakova, I.L.; Kilpio, T.; Leino, A.R.; Kordás, K.; Eränen, K.; Mäki-Arvela, P.; Murzin, D.Y. Step changes and deactivation behaviour in the continuous decarboxylation of stearic acid. *Ind. Eng. Chem. Res.* **2011**, *50*, 11049–11058. [[CrossRef](#)]
21. Madsen, A.T.; Rozmysłowicz, B.B.; Mäki-Arvela, P.; Simakova, I.L.; Eränen, K.; Murzin, D.Y.; Fehrmann, R. Deactivation in continuous deoxygenation of C₁₈ fatty feedstock over Pd/Subunit. *Top. Catal.* **2013**, *56*, 714–724. [[CrossRef](#)]
22. Simakova, I.; Simakova, O.; Mäki-Arvela, P.; Simakov, A.; Estrada, M.; Murzin, D.Y. Deoxygenation of palmitic and stearic acid over supported Pd catalysts: Effect of metal dispersion. *Appl. Catal. A* **2009**, *355*, 100–108. [[CrossRef](#)]
23. Mäki-Arvela, P.; Kubickova, I.; Snåre, M.; Eränen, K.; Murzin, D.Y. Deoxygenation of fatty acids and their derivatives. *Energy Fuels* **2007**, *21*, 30–41. [[CrossRef](#)]
24. Lestari, S.; Mäki-Arvela, P.; Bernas, H.; Simakova, O.; Sjöholm, R.; Beltramini, J.; Max Lu, G.Q.; Myllyoja, J.; Simakova, I.; Murzin, D.Y. Catalytic deoxygenation of stearic acid in a continuous reactor over a mesoporous carbon supported Pd catalyst. *Energy Fuels* **2009**, *23*, 3842–3845. [[CrossRef](#)]
25. Fu, J.; Lu, X.; Savage, P.E. Catalytic hydrothermal deoxygenation of palmitic acid. *Energy Environ. Sci.* **2010**, *3*, 311–317. [[CrossRef](#)]
26. Ford, J.P.; Immer, J.G.; Lamb, H.H. Palladium catalysts for fatty acid deoxygenation: Influence of the support and fatty acid chain length on decarboxylation kinetics. *Top. Catal.* **2012**, *55*, 175–184. [[CrossRef](#)]

27. Kubička, D.; Bejblová, M.; Vlk, J. Conversion of vegetable oils into hydrocarbons over CoMo/MCM-41 catalysts. *Top. Catal.* **2010**, *53*, 168–178. [[CrossRef](#)]
28. Lestari, S.; Mäki-Arvela, P.; Eränen, K.; Beltramini, J.; Max Lu, C.Q.; Murzin, D.Y. Diesel-like hydrocarbons from catalytic deoxygenation of stearic acid over supported Pd nanoparticles on SBA-15 catalysts. *Catal. Lett.* **2010**, *134*, 250–257. [[CrossRef](#)]
29. Duan, J.; Han, J.; Sun, H.; Chen, P.; Lou, H.; Zheng, X. Diesel-like hydrocarbons obtained by direct hydrodeoxygenation of sunflower oil over Pd/Al-SBA-15 catalysts. *Catal. Commun.* **2012**, *17*, 76–80. [[CrossRef](#)]
30. Peng, B.; Yao, Y.; Zhao, C.; Lercher, J.A. Upgrading pyrolysis oil over Ni/HZSM-5 by cascade reactions. *Angew. Chem. Int. Ed.* **2012**, *124*, 2114–2117. [[CrossRef](#)]
31. Murata, K.; Liu, Y.; Inaba, M.; Takahara, I. Production of synthetic diesel by hydrotreatment of jatropha oils using Pt-Re/HZSM-5 catalyst. *Energy Fuels* **2010**, *24*, 2404–2409. [[CrossRef](#)]
32. Serrano, D.P.; Escola, J.M.; Briones, L.; Arroyo, M. Selective hydrodecarboxylation of fatty acids into long chain hydrocarbons catalyzed by Pd/Al-SBA-15. *Microporous Mesoporous Mater.* **2019**, *280*, 88–96. [[CrossRef](#)]
33. Li, J.; Li, X.; Zhou, G.; Wang, W.; Wang, C.; Komarneni, S.; Wang, Y. Catalytic fast pyrolysis of biomass with mesoporous ZSM-5 zeolites prepared by desilication with NaOH solutions. *Appl. Catal. A* **2014**, *470*, 115–122. [[CrossRef](#)]
34. Botas, J.A.; Serrano, D.P.; García, A.; Ramos, R. Catalytic conversion of rapeseed oil for the production of raw chemicals, fuels and carbon nanotubes over Ni-modified nanocrystalline and hierarchical ZSM-5. *Appl. Catal. B* **2014**, *145*, 205–215. [[CrossRef](#)]
35. Serrano, D.P.; Aguado, J.; Escola, J.M.; Rodríguez, J.M.; Peral, A. Hierarchical zeolites with enhanced textural and catalytic properties synthesized from organofunctionalized seeds. *Chem. Mater.* **2006**, *18*, 2462–2464. [[CrossRef](#)]
36. Serrano, D.P.; Escola, J.M.; Briones, L.; Arroyo, M. Hydroprocessing of the LDPE thermal cracking oil into transportation fuels over Pd supported on hierarchical ZSM-5 catalyst. *Fuel* **2017**, *206*, 190–198. [[CrossRef](#)]
37. Serrano, D.P.; Pinnavaia, T.J.; Aguado, J.; Escola, J.M.; Peral, A.; Villalba, L. Hierarchical ZSM-5 zeolites synthesized by silanization of protozeolitic units: Mediating the mesoporosity contribution by changing the organosilane type. *Catal. Today* **2014**, *227*, 15–25. [[CrossRef](#)]
38. Wang, C.; Xu, J.; Qi, G.; Gong, Y.; Wang, W.; Gao, P.; Wang, Q.; Feng, N.; Liu, X.; Deng, F. Methylbenzene hydrocarbon pool in methanol-to-olefins conversion over zeolite H-ZSM-5. *J. Catal.* **2015**, *332*, 127–137. [[CrossRef](#)]
39. Chung, Y.-M.; Mores, D.; Weckhuysen, B.M. Spatial and temporal mapping of coke formation during paraffin and olefin aromatization in individual H-ZSM-5 crystals. *Appl. Catal. A* **2011**, *404*, 12–20. [[CrossRef](#)]
40. Dai, S.; Zhou, S.; Zhang, W.; Chen, C. Systematic investigation of ligand steric effects on α -Diimine Palladium catalyzed olefin polymerization and copolymerization. *Macromolecules* **2016**, *49*, 8855–8862. [[CrossRef](#)]
41. Netalkar, S.P.; Budagumpi, S.; Abdallah, H.H.; Netalkar, P.P.; Revankar, V.K. Sterically modulated binuclear bis α -diimine Pd(II) complexes: Synthesis, characterization, DFT studies and catalytic behaviour towards ethylene oligomerization. *J. Mol. Struct.* **2014**, *1075*, 559–565. [[CrossRef](#)]
42. Karatun, O.N.; Dorogochinskii, A.Z. Oligomerization and aromatization of propylene. Pd-containing catalysts on high-silica zeolite. *Chem. Technol. Fuels Oils* **2000**, *36*, 416–420. [[CrossRef](#)]
43. Wang, J.; Wang, L.; Yu, H.; Ullah, R.S.; Haroon, M.; Zain-ul-Abdin, X.; Khan, R.U. Recent progress in ethylene polymerization catalysed by Ni and Pd catalysts. *Eur. J. Inorg. Chem.* **2018**, 1450–1468. [[CrossRef](#)]
44. Puthiaraj, P.; Kim, K.; Ahn, W.S. Catalytic transfer hydrogenation of bio-based furfural by palladium supported on nitrogen-doped porous carbon. *Catal. Today* **2019**, 49–58. [[CrossRef](#)]
45. Alam, M.I.; Khan, T.S.; Haider, M.A. Alternate biobased route to produce I-decalactone: Elucidating the role of solvent and hydrogen evolution in catalytic transfer hydrogenation. *ACS Sustain. Chem. Eng.* **2019**, *7*, 2894–2898. [[CrossRef](#)]

46. Shafaghat, H.; Rezaei, P.S.; Daud, W.M.A.W. Using decalin and tetralin as hydrogen source for transfer hydrogenation of renewable lignin-derived phenolics over activated carbon supported Pd and Pt catalysts. *J. Taiwan Inst. Chem. Eng.* **2016**, *65*, 91–100. [[CrossRef](#)]
47. Muzart, J. Pd-catalyzed hydrogen transfer reactions from alcohols to C=C, C=O and C=N bonds. *Eur. J. Org. Chem.* **2015**, *26*, 5693–5707. [[CrossRef](#)]



© 2019 by the authors. Licensee MDPI, Basel, Switzerland. This article is an open access article distributed under the terms and conditions of the Creative Commons Attribution (CC BY) license (<http://creativecommons.org/licenses/by/4.0/>).